PCCP

Accepted Manuscript

This is an *Accepted Manuscript*, which has been through the Royal Society of Chemistry peer review process and has been accepted for publication.

Accepted Manuscripts are published online shortly after acceptance, before technical editing, formatting and proof reading. Using this free service, authors can make their results available to the community, in citable form, before we publish the edited article. We will replace this *Accepted Manuscript* with the edited and formatted *Advance Article* as soon as it is available.

You can find more information about *Accepted Manuscripts* in the **Information for Authors**.

HSO$_3$Cl: A Prototype Molecule for Studying OH-stretching Overtone Induced Photodissociation

Juvenal Yosa Reyes[1,2,#], Sebastian Brickel [1,#], Oliver Unke[1], Tibor Nagy[1,3], Markus Meuwly[1,*]

[1]Department of Chemistry, University of Basel, Klingelbergstrasse 80, Basel, Switzerland

[2]Industrial and Systems Engineering Department, National

University Bogotá, Carrera 45 # 26-85, Bogotá, Colombia

[3]IMEC, RCNS, Hungarian Academy of Sciences, Magyar tudósok körútja 2., Budapest, Hungary

[#]These authors contributed equally to this work

(Dated: January 18, 2016)

Abstract

Vibrationally induced photodissociation in sulfurochloridic acid (HSO$_3$Cl) is found to be a viable process to form SO$_3$ and HCl from excitations of the OH-stretching overtone starting at $\nu_{OH} = 4$. Reactive molecular dynamics simulations on a fully-dimensional potential energy surface fitted to MP2 calculations show that hydrogen transfer and HCl elimination compete with one another on the nanosecond time scale. For excitation with 5 and 6 quanta in the OH-stretch direct elimination of HCl is the dominant process on the several hundred picosecond time scale. At longer times, HCl formation is preceded by intramolecular hydrogen transfer and concomitant excitation of torsional degrees of freedom. As HSO$_3$Cl is a suitable proxy for H$_2$SO$_4$, which is relevant for weather and climate in the upper atmosphere, it is concluded that vibrationally induced photodissociation is a possible mechanism for H$_2$SO$_4$ decomposition. Final state energy distributions for different internal degrees of freedom are predicted which should be observable in laboratory measurements.

1

I. INTRODUCTION

The photochemistry of halogen- and sulfur-containing compounds which are involved in acid rain and aerosol formation in the tropo- and stratosphere, are of significance to the chemistry of the atmosphere. This led to extensive studies, both experimental and theoretical, concerning a wide range of chemical reactions relevant for climate and weather.[1] In 1982 Hofmann and Rosen suggested that the formation of condensation nuclei from sulfur compounds is dominated by photochemical processes and they related the periodic de- and increase of these particles to the cycle of polar night and day around the poles.[2] This seasonal change in the solar radiation affects directly the stratospheric aerosol layer by altering the rate of photochemical reactions of sulfur-containing compounds and thereby influences the climate and weather.

One of the central sulfur compounds in the stratospheric aerosol layer is sulfuric acid (H_2SO_4).[2–4] Sources for H_2SO_4 in the atmosphere are generally sulfur-containing compounds which are primarily emitted as dimethyl sulfide (DMS) and sulfur dioxide (SO_2).[5–9] These compounds are oxidized in the atmosphere to form sulfur trioxide (SO_3) and subsequently hydrolyzed to H_2SO_4.[10,11] Among other, stratospheric sulfate aerosol has a global dimming effect in the atmosphere and increases the number of aerosol particles which can limit the effect and impact of global warming.[12] This makes H_2SO_4 a suitable candidate in climate engineering projects.[13] Additionally, the formation of a layer of dispersed aerosol found at high altitudes (between 15 to 35 km) which influences stratospheric ozone depletion, the so called Junge layer[14], can be explained by the cycling between SO_2 and H_2SO_4.[15–17]

Sulfur-containing compounds, in particular the interplay between H_2SO_4 and SO_2, are important in the formation of atmospheric aerosols. The observed anomalous enhancement in particle concentration during springtime and the finding that the SO_2 concentration from photolysis of H_2SO_4 is constant or increases with altitude[16] suggested that at high altitudes photolysis of sulfuric acid is the source of SO_2.[18] However, experimental and computational investigations were unable to find the electronic absorption spectrum of H_2SO_4 down to 140 nm.[19–23] According to Lane and Kjaergaard[24] the lowest calculated electronic transition is at 139 nm. Hence, UV excitation from solar photons is improbable to produce SO_2 from H_2SO_4 and an alternative reaction mechanism for H_2SO_4 decomposition was required.

Experimentally and computationally it was previously found that vibrational excitation can induce bond-selective photodissociation.[25–27] It was therefore proposed that highly-excited OH-stretching states can lead to dissociation of H_2SO_4.[18] The vibrational spectrum of H_2SO_4 in the near-infrared and visible regions has been intensely studied, both experimentally[19,28–31] and computationally.[22,23,31–33] Nevertheless it was not possible to experimentally verify that vibrational overtone-induced photodissociation is operative in H_2SO_4. This is due to particular experimental difficulties involving this species. By mixing known vapor flows of H_2O and SO_3 at elevated temperature (400-500 K) H_2SO_4 can be generated in the vapor phase ($H_2O + SO_3 \longrightarrow H_2SO_4$).[19] However, H_2SO_4 has an extremely low vapor pressure, and exists in equilibrium with H_2O and SO_3 in the gas phase. Therefore this approach leads to difficulties in distinguishing the reactants and products.[29,34]

Because of the above mentioned difficulties and the widespread relevance of the atmospheric decomposition of sulfates, sulfuric acid derivatives have been considered to provide experimental evidence for characterizing OH-stretching induced dissociation in the gas phase.[29,34,35] Such candidate compounds are sulfurochloridic acid (HSO_3Cl) and sulfurofluoridic acid (HSO_3F) which are related to H_2SO_4[29,34], but experimentally more amenable. The dissociation energy to eliminate HCl and HF from HSO_3Cl and HSO_3F, respectively, are similar to those of H_2O from H_2SO_4 (32-40 kcal/mol).[34] Using a simple one-dimensional anharmonic oscillator local model, the overtone spectra of sulfuric acid derivatives have been computed, which found that excitation of the OH-stretching transition with $\Delta v \geq 4$ and $\Delta v \geq 5$, will provide sufficient energy for photodissociation of HSO_3Cl and HSO_3F, respectively.[29,34,35] Finally, *ab initio* molecular dynamics (MD) simulations have demonstrated that the decomposition of these derivatives, similar to what has been proposed to H_2SO_4, is possible *via* excitation of higher OH-stretching overtone transitions.[29,34] At the semi-empirical PM3 level, it was found that for HSO_3Cl, excitation of $v \geq 4$, or $v \geq 5$ (PM3) can induce the elimination reaction.[34] For photodissociation of HSO_3F excitation of the $v \geq 7$ OH-stretching state is necessary with PM3, whereas excitation of the $v \geq 5$ overtone is sufficient at the MP2/TZP level.[34] The average reaction time for both, HSO_3Cl and HSO_3F, was of the order of 10 ps, determined from 32 trajectories.[34] However, previous reactive MD simulations on H_2SO_4 have demonstrated that for converged reaction time distributions several thousand trajectories are required.[32,33]
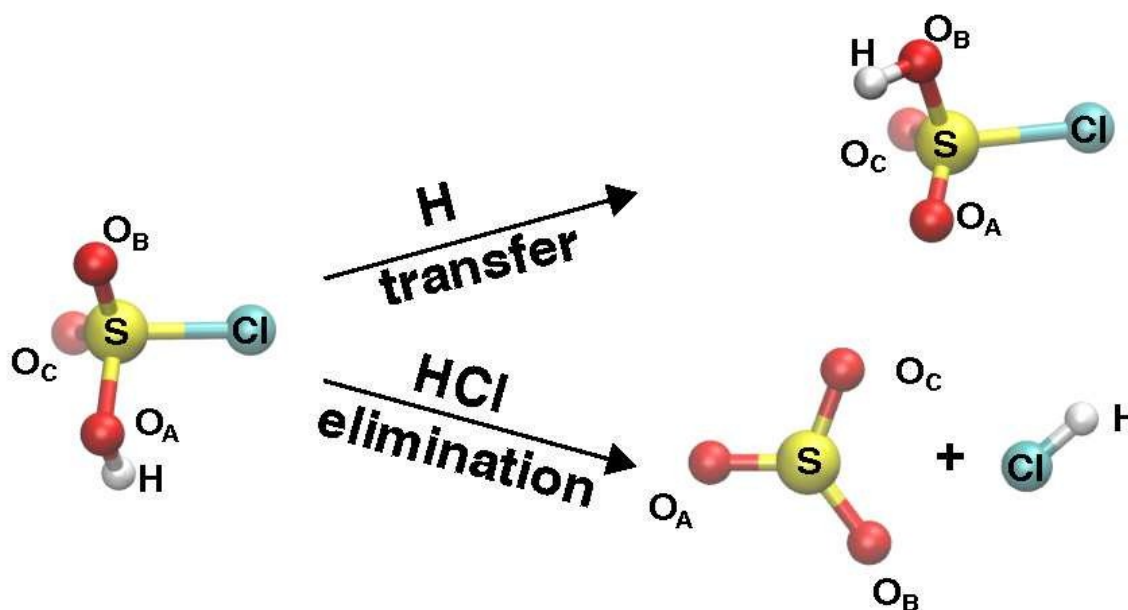
FIG. 1: Graphical representation of the two possible reaction pathways involving HSO_3Cl considered here. Top trace: intramolecular H-transfer ($O_AH \rightarrow O_BH$), bottom trace: HCl elimination.

In order to characterize and understand the dynamics of vibrationally induced decomposition of HSO_3Cl and to guide future experimental efforts, Multi-Surface Adiabatic Reactive Molecular Dynamics (MS-ARMD) simulations were carried out.[36] This method is capable of treating multiple reaction pathways based on force fields to describe the adiabatic potential energy surface and the classical reaction dynamics of the system, and to run and analyze a statistically significant number of trajectories. Here, the dynamics on a fully dimensional reactive potential energy surface (PES) capable of following intramolecular H-transfer and HCl elimination in HSO_3Cl (see Figure 1) is investigated. This provides the information to analyze the yields and determine rate coefficients along with the final state energy distribution in the products as a function of the vibrational overtone that was initially excited. This information can be directly compared with forthcoming experiments.

II.   REACTIVE MOLECULAR DYNAMICS SIMULATIONS

The global PES for the reactions of HSO_3Cl is based on reference electronic structure calcula-
tions at the MP2/6-311G++(2d,2p) level of theory. All *ab initio* calculations were performed with
Gaussian09[37]. The energy at the equilibrium geometry of HSO_3Cl was chosen as the global zero
of energy. The functional form of the force field which describes the HSO_3Cl, SO_3 and HCl states,
including the $SO_3 \cdots HCl$ van der Waals complex has the following form:

$$
\begin{aligned}
V(\mathbf{x}) = & \sum_{\text{bonds}} D_e (1 - e^{-\beta(r-r_0)})^2 + \sum_{\text{angles}} K_\theta (\theta - \theta_0)^2 \\
& + \sum_{\text{Urey-Bradley}} K_{\text{UB}} (S - S_0)^2 \sum_{\text{dihedral}} H_\phi (1 + \cos(n\phi - \delta)) \\
& + \sum_{\text{impropers}} K_\omega (\omega - \omega_0)^2 \\
& + \sum_{ij} \left\{ \frac{n\varepsilon_{ij}}{m-n} \left[\left(\frac{r_{\min,ij}}{r_{ij}} \right)^m - \frac{m}{n} \left(\frac{r_{\min,ij}}{r_{ij}} \right)^n \right] + \frac{q_i q_j}{4\pi\varepsilon_0 r_{ij}} \right\}
\end{aligned}
\tag{1}
$$

where r_0 is the equilibrium bond distance, D_e is the dissociation energy, and β controls the
steepness and width of the Morse potential.[36] Additionally a generalized Lennard-Jones potential
($\sum_{ij}$) is included, in order to better represent the van der Waals interaction between atoms in the
reactive region.[36] The PESs of the three molecules (HSO_3Cl, SO_3 and HCl) together with the van
der Waals complex ($SO_3 \cdots HCl$) were parameterized independently. Specifically, the HSO_3Cl
state is described by all terms in equation 1, whereas for SO_3 only bonds, angles, Urey-Bradley,
improper dihedrals and non-bonded terms, are needed. For HCl a bonded term and non-bonded
terms (for the van der Waals complex) were required. For the reactive PES of the overall system
the individual PESs were joined into a global reactive PES using the MS-ARMD switching
method and were combined with Gaussian × polynomial (GAPOs) functions which provide
the necessary flexibility to model the barrier crossing region.[36] The interpolation of the PESs is
accomplished through energy-dependent weights $w_i(E)$.[36]

Details of the fitting are described in the Supplementary Information. Optimization of the force
field yields parameters for the global reactive PES which allows to follow the H-transfer and
HCl elimination reactions. The root-mean-square deviations (RMSD) between *ab initio* reference
energies and FF energies are 0.22 and 0.29 kcal/mol, for the barrier region of HCl elimination and
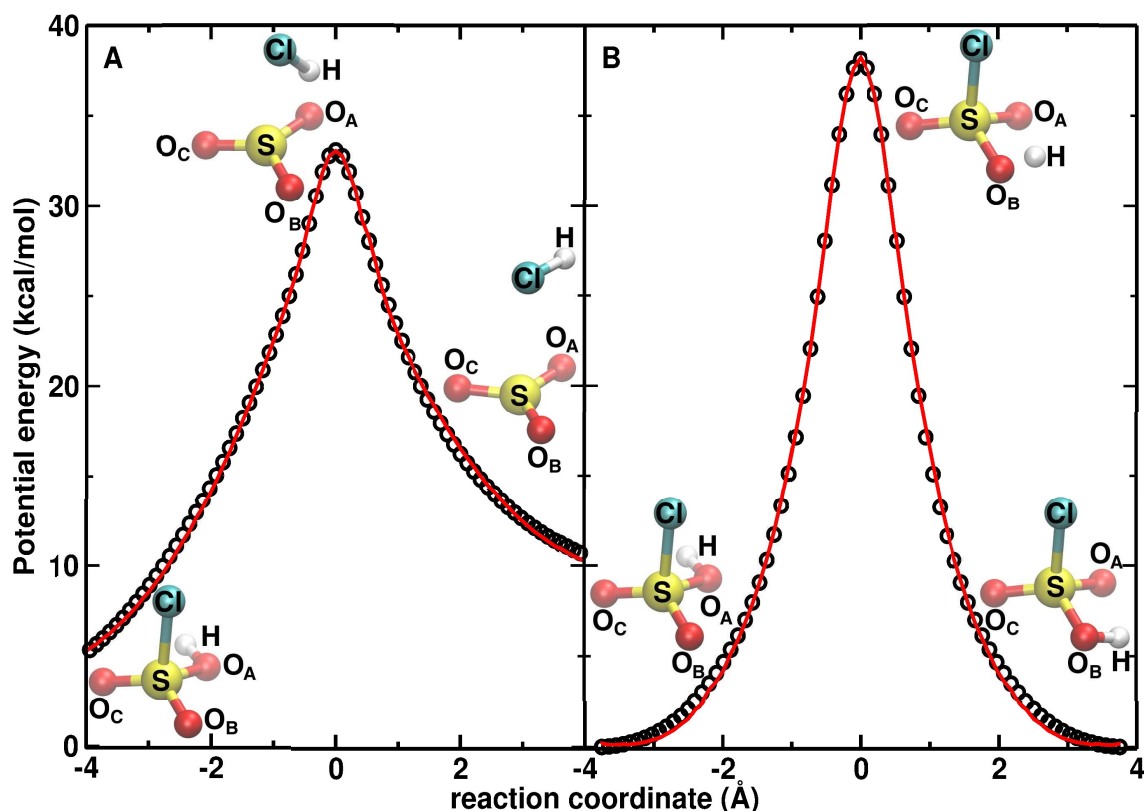intramolecular H-transfer, respectively, see red curves in Figure 2 A and B.

FIG. 2: Minimum Energy Path for A) HCl elimination and B) intramolecular H-transfer. Black circles represent the *ab initio* reference energies, red curves represent the FF energies including GAPOs.

The RMSD between the energy-minimized structures at the MP2/6-311G++(2d,2p) level and using the force field is 0.004 Å whereas for the $SO_3 \cdots HCl$ van der Waals complex the RMSD is 0.053 Å. A comparison of equilibrium bond lengths, angles and dihedral angles is provided in Table S-I (Supplementary Information). The geometries in Table S-I are also in good agreement with those computed using MP2/TZP (Dunning's triple-ζ+ polarization).[34] In addition, a normal mode analysis was performed in order to compare the experimentally observed vibrational frequencies with those from the MP2 and FF calculations, see Table S-II (Supplementary Information). The average differences between experimental,[38,39] MP2 and FF harmonic frequencies for HSO_3Cl are 4.56 and 4.71 cm^{-1}, respectively which establishes the quality of the force field.

Particularly relevant for the reaction rates are the barrier heights. The MP2/6-311G++(2d,2p)

computed values are close to those determined previously using CCSD(T)/aug-cc-pV(T+d)Z[34]. For HCl elimination the value of 34.0 kcal/mol[34] compares with 33.1 kcal/mol from the present study. As the final global PES provides a good description of the equilibrium geometry, the harmonic frequencies and the barrier heights compared to results from *ab initio* calculations, the reactive PES is considered to be parameterized in a meaningful way. Contrary to an *ab initio* MP2/6-311G++(2d,2p) single point calculation, the reactive FF requires a fraction of the computational cost, which is highly relevant for dynamical studies.

The quality of the reactive PES is shown in Figure 3. It provides a comparison between the energies of the reference MP2 calculations compared with the FF. For the representative structures from an equilibrium simulation at 300 K, the IRCs (HCl elimination and intramolecular H-transfer, obtained from individual scans) and the $HCl+SO_3$ van der Waals complex the absolute average difference between the reference MP2 energies and the FF is 0.52 kcal/mol.

All MD simulations were carried out with CHARMM[40] with provisions for bond-breaking and bond-formation through MS-ARMD[36]. Starting from a geometry optimized structure of HSO_3Cl, the system was heated to 300 K. The equations of motion were propagated with the leapfrog Verlet algorithm with a time step of $\Delta t = 0.1$ fs during 40 ps and equilibrated for 40 ps, followed by 250 ns of free dynamics simulations (i.e. constant energy NVE), where a structure was collected every 50 ps. The small time step is required to appropriately follow the rapid dynamics of the H-atom.

The nonequilibrium state was prepared by scaling the instantaneous velocity vector at the moment of excitation along the normal mode of interest which is the ν_{OH} mode in the present case. Similar to the situation in H_2SO_4 this mode has predominantly local OH-stretching character. Such a scheme, which modifies only the kinetic energy, has already been successfully employed for H_2SO_4 and for studying proton transfer in small H-bonded complexes.[32,33,41] An alternative approach is to change both, kinetic and potential energy, by modifying positions and velocities.[42] While changing only the kinetic energy can lead to accelerated redistribution of vibrational energy, modification of positions and momenta requires a short equilibration period to avoid artifacts due to close proximity of atoms which may be a potential drawback in this approach.[42] Nonequilibrium excitation of a thermal ensemble as described above is closest to the situation

encountered in a laboratory experiment and was therefore preferred over generating quasiclassical (QCT) nonequilibrium initial conditions.

The OH stretch potential can be realistically described by a Morse potential for which the exact energy levels are known. The excitation energies for $\nu_{OH} = 3, 4, 5,$ and 6 are: 11699 cm^{-1} (33.3 kcal/mol), 14760 cm^{-1} (42.2 kcal/mol), 17662 cm^{-1} (50.5 kcal/mol), and 20405 cm^{-1} (58.3 kcal/mol) using $D_e = 122.88$ kcal/mol and $\beta = 2.11$ Å^{-1} from the current O-H bond in the MS-ARMD potential. An alternative means to select initial conditions is described in the Results section.

III. RESULTS

From 5000 independent trajectories with a maximum simulation time of 2.5 ns, more than 90% of the trajectories were reactive when $\nu_{OH} = 5$ or 6 are excited (see Figure 4). Both processes, (I) HCl elimination without prior H-transfer (dashed line), called direct, and (II) HCl elimination preceded by intramolecular H-transfer (dotted dashed line), called indirect, are observed. Direct HCl elimination is found for 0.2, 10.4, 28.5, and 42.8% of the cases for $\nu_{OH} = 3, 4, 5,$ and 6. HCl elimination preceded by intramolecular H-transfer was observed for 4.2, 62.0, and 54.9% of the cases for $\nu_{OH} = 4, 5$ and 6 whereas for $\nu_{OH} = 3$ this reaction channel was not observed. Intramolecular H-transfer without HCl elimination within 2.5 ns (leading to complete intramolecular vibrational energy redistribution (IVR), which strongly decreases the decay probability) was found for 10.2, 35.3, 7.3, and 0.08% of the cases for $\nu_{OH} = 3, 4, 5,$ and 6.

For excitation with $\nu_{OH} = 5$ and 6 decomposition occurs on the hundred picosecond time scale. Overall 50% of the trajectories show HCl elimination within 500 ps for excitation with $\nu_{OH} = 6$. For $\nu_{OH} = 5$ the proportion is around 34% after 500 ps. The majority of these trajectories that show decomposition for $\nu_{OH} = 5$ and 6 lead to direct HCl elimination, without previous H-transfer. On a longer time scale indirect elimination becomes dominant, as some time is required for the "hydrogen hopping". For $\nu_{OH} = 3$ and 4 decomposition of activated HSO$_3$Cl continues and much longer simulation times, particularly for the excitation with 3 quanta, would be required until all potential elimination reactions have occurred. It is worthwhile to mention that
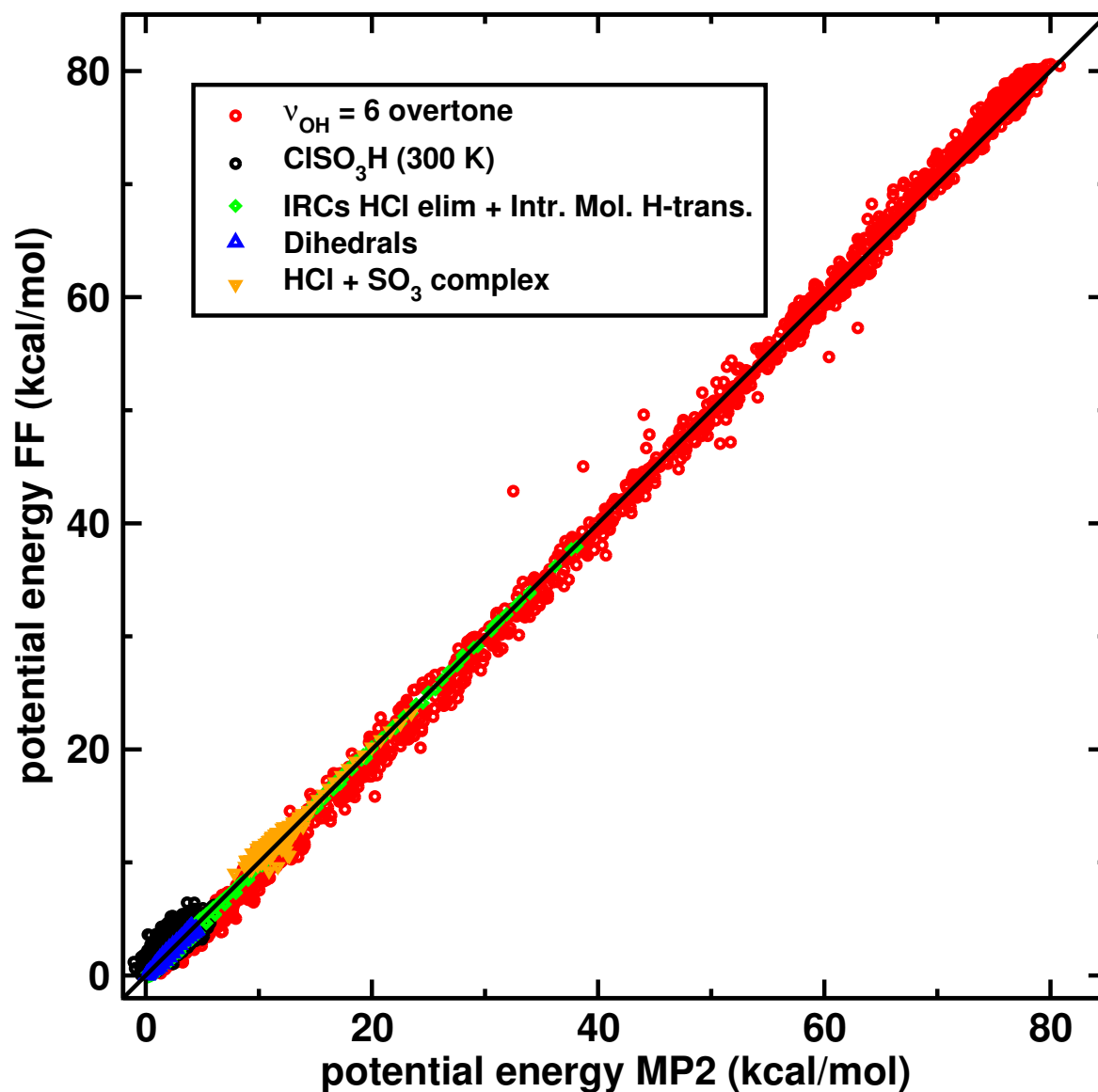
8

FIG. 3: Quality of the reactive PES. The reference data points are calculated at the MP2/6-311G(d,p) level of theory and compared to the parameterized surface.

the mean collision time was estimated to be around 130 ns.[33] However, multiple 1000 simulations on this time scale become computationally prohibitive even with an empirical force field. The effect of deuteration was assessed by running 5000 trajectories for DSO_3Cl with $\nu_{OD} = 5$ which corresponds to 13546 cm^{-1} (36.2 kcal/mol). Within 2.5 ns, 2 % of these trajectories showed DCl elimination, nearly all of them following process I. Hence, for the deuterated species much higher
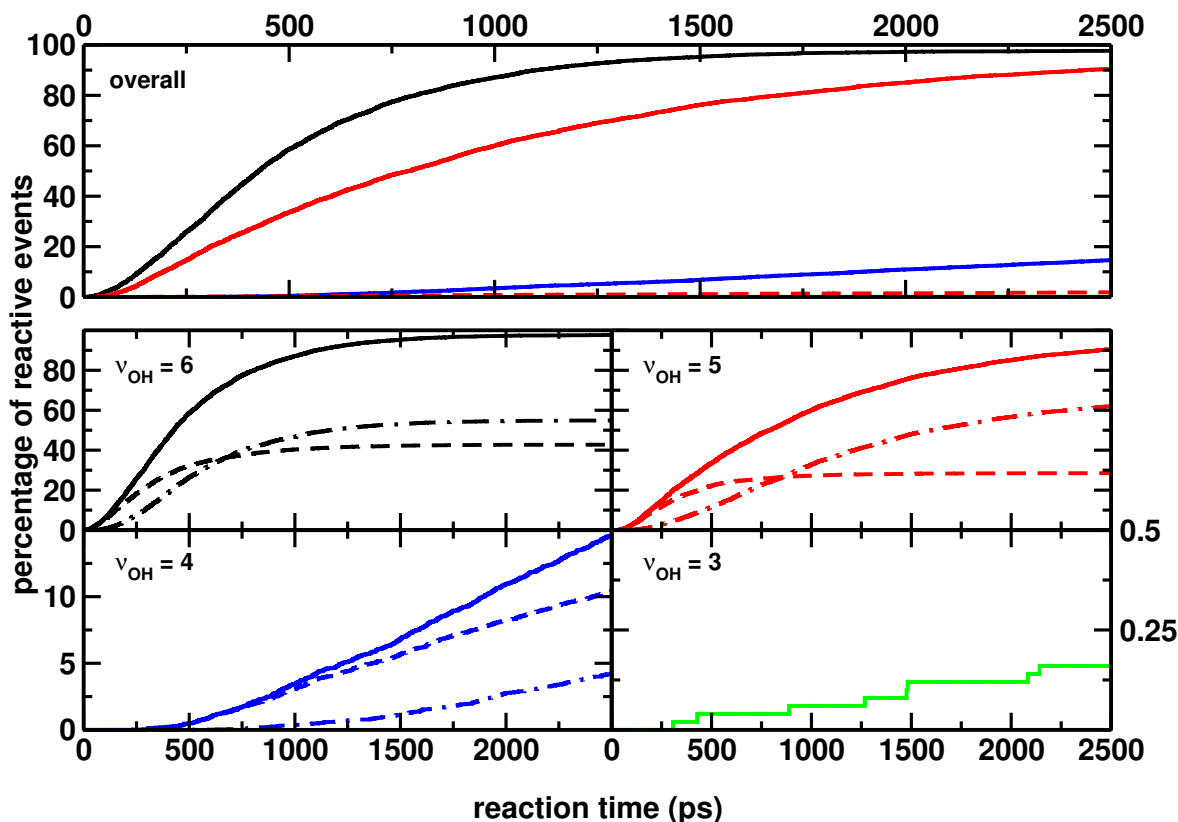
FIG. 4: Percentage of HCl elimination as a function of simulation time. Top panel: Total number of reactive events (direct HCl elimination + HCl elimination preceded by intramolecular H-transfer). Green, blue, red and black curves correspond to excitation of $\nu_{OH} = 3$, 4, 5 and 6, respectively. The red dashed curve corresponds to DCl elimination in DSO_3Cl with $\nu_{OD} = 5$. Bottom panels: Total number of reactive events (solid), direct HCl elimination (dashed), and HCl elimination preceded by intramolecular H-transfer (dotted dashed) for $\nu_{OH} = 3$, 4, 5 and 6 in the same color code as in the top panel.

vibrational excitations are required for photodissociation which leads to a smaller cross section due to reduced overlap of the initial and final vibrational states than for the hydrogenated species.

Compared with a previous study on H_2SO_4[33] considerable differences in the number of reactive events for excitation with 5 or 6 quanta are found. For HSO_3Cl the percentage of trajectories which lead to HCl elimination (yield) is $\approx 60\%$ for $\nu_{OH} = 5$ after 1 ns, which is markedly increased compared to 25% in H_2SO_4 for the same OH stretching overtone within 1 ns, even though the barrier in H_2SO_4 is slightly lower. For sulfuric acid direct elimination was the

dominant process for all excitation levels. Only 3.4% and 12.2% of the trajectories in H_2SO_4 for 5 and 6 quanta, respectively, were found to proceed via indirect elimination.[33] This can be explained by the fact that in H_2SO_4 direct elimination occurs more rapidly than in HSO_3Cl. As an example, for $v_{OH} = 5$ the number of direct eliminations levels out (i.e. all eliminations on longer time scales are preceded by intramolecular H-transfer) after 300 ps in H_2SO_4 compared to 500 ps in HSO_3Cl.

The higher product yield for the same time after excitation (see previous paragraph) can be explained, in part, by the fact that the excitation energy in HSO_3Cl is higher than in H_2SO_4, which speeds up the elimination reaction: for $v_{OH} = 5$ the difference between H_2SO_4 (47.2 kcal/mol) and HSO_3Cl (50.5 kcal/mol) is 3.3 kcal/ mol whereas the barrier heights for H_2O and HCl elimination only differ by 1.1 kcal/mol, respectively. Furthermore, in H_2SO_4 two hindered rotors (HOSO) need to be in a relative position allowing for H_2O elimination, whereas for HCl elimination in HSO_3Cl only one such dihedral exists. On the other hand, the number of ways in which H_2O elimination can occur is larger (two -OH groups) for H_2SO_4 compared to HCl elimination in HSO_3Cl. Hence both, energetic and entropic factors contribute to the differences in the product yields for the two systems. However, a detailed comparative analysis of these effects is outside the scope of the present work.

Most relevant for future experiments is the final state analysis of the products, which is also an observable.[43] In order to characterize the energy distribution after vibrational excitation and subsequent HCl elimination, the translational, rotational and vibrational energies in the reaction products were determined following established methodologies, as described in the Supplementary Information. The analysis was carried out for all trajectories tat experienced HCl elimination within 2.5 ns for $v_{OH} = 4$, 5, and 6. The analysis for $v_{OH} = 3$ was excluded due to the small number of reactive events. Final state analysis starts after HCl elimination when the sulfur-chlorine distance exceeds 20 Å. Trajectories were then continued for an additional 5 ps during which 500 snapshots for each trajectory were collected and analyzed. Translational, rotational, and vibrational energies as well as the total angular momentum were computed for every snapshot. Rotational and vibrational energies were averaged over the 500 snapshots. From these averages the probability distributions of the averaged values were determined.

Figure 5 shows the distribution of translational, rotational, and vibrational energies of the products for $\nu_{OH} = 4$ (blue), 5 (red), and 6 (black). The peak position of translational energies differ by less than 3 kcal/mol for the three excitation levels. For SO_3 a maximum peak for excitation with all quanta is found at about 5 kcal/mol. Rotational energy distributions for HCl peaks at about 3.5 kcal/mol (corresponding to a maximum angular momentum of $j = 11$), with a difference of the peak position of less than 1 kcal/mol. For SO_3 the rotational energy shifts towards higher energies for lower ν_{OH}. The vibrational energies show similar behavior for HCl and SO_3. In both cases the vibrational energy distribution widens for higher overtone excitation. For SO_3 the maximum peaks at around 11, 15, and 19 kcal/mol for $\nu_{OH} = 4$, 5 and 6 respectively.

The $j-$distribution (Figure S-III (Supplementary Information)) for SO_3 exhibits a single maximum around $j = 60$ to 70 for all investigated excitations. Contrary to that, for HCl a slight bimodal $j-$distribution for higher vibrational excitations, specifically for $\nu_{OH} = 6$ is found. The two peaks can be assigned to the direct and indirect product channels. Direct elimination, with a peak around $j = 10$, is associated with higher vibrational energy, whereas indirect elimination leads to a higher $j-$value (around $j = 12$).

An alternative method to characterize final states from MD simulations, in particular for vibrational degrees of freedom, is the Gaussian binning procedure.[44] This was applied to the diatomic product as this would also be most relevant from an experimental perspective. Gaussian binning involves assigning larger weights to final states with fractional vibrational quantum numbers x_i closer to an integer value n_i. For the present case of a diatomic and following Ref.[44] the weight is $w = \sqrt{\beta}e^{-\beta(x-n)^2}$ where x and n are the fractional and integer quantum numbers of HCl in the product state, respectively. The parameter β should be chosen sufficiently large in order to reduce weights of final states near half-integer values and was $\beta = 20$ in the present case. For excitation of HSO_3Cl with $v = 4$ the final state population for the HCl stretching mode is 43 % ($v_{HCl} = 0$), 30 % ($v_{HCl} = 1$), 18 % ($v_{HCl} = 2$), and 9 % ($v_{HCl} \geq 3$). This only differs marginally from weighting all final states equally ($w = 1$) and supports the final state analysis discussed above.

In order to validate the results, an alternative method to generate initial conditions was employed. Instead of starting from an equilibrium ensemble at 300 K, energies were drawn from a Maxwell-Boltzmann distribution using Metropolis Monte Carlo (MC) sampling and initial
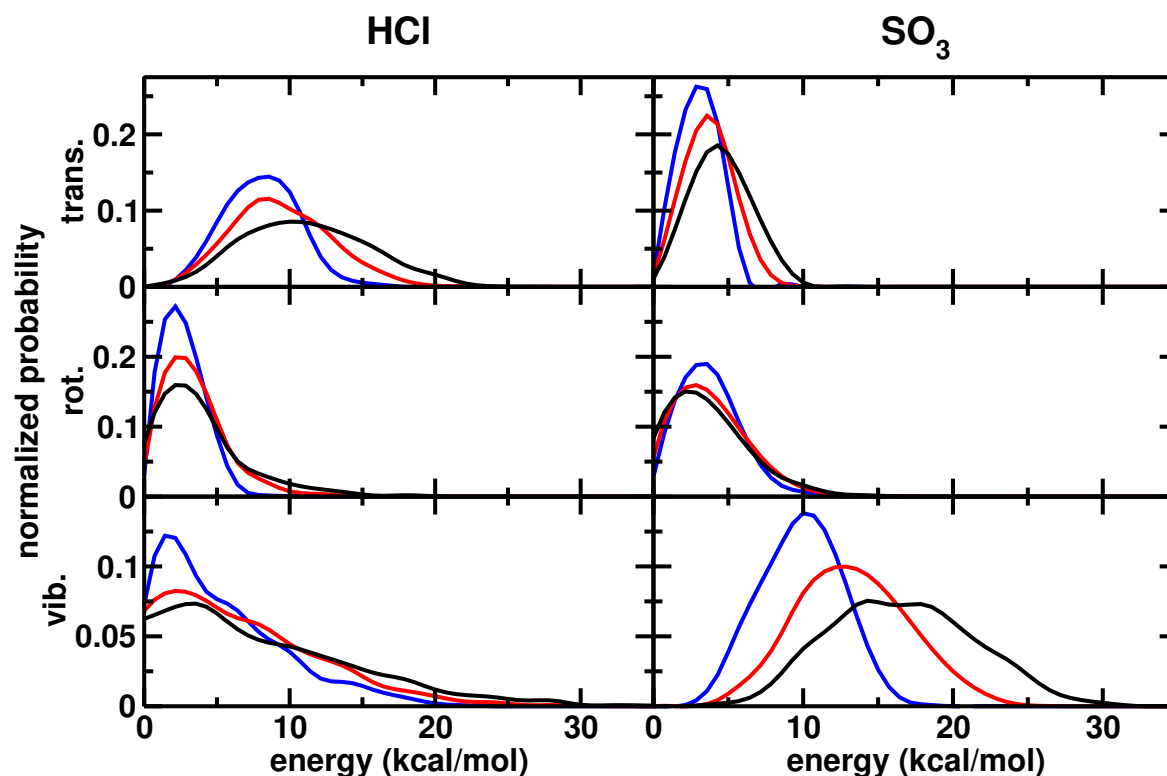
FIG. 5: Final state analysis for HCl and SO$_3$. Blue, red, and black curves correspond to excitation of $\nu_{OH} = 4$, 5 and 6, respectively. The abbreviations trans., rot. and vib. stand for the translational, rotational, and vibrational energy, respectively.

conditions generated according to an algorithm developed by Schranz *et al.*[45]. For each drawn energy E, spatial coordinates are selected from the final state of a Markov chain generated by a Metropolis-type procedure.[46] Then, random momentum vectors are generated from a Gaussian distribution for each atom. Finally, the momentum vectors are rescaled such that the total kinetic energy $T = E - V$, where V is the potential energy of the generated configuration. For convenience, all generated conditions were transformed to a center-of-momentum frame. The potential energy distribution for the two different ensembles are similar to one another. The distribution of the potential energy for the ensembles generated from the MC sampling shows a maximum peak slightly closer to $\frac{15}{2}k_B T$, which is the thermodynamic value.

Figure 6 shows the decomposition probability for 1000 trajectories generated with the MC method. The excitation of the OH bond was applied in the same way as for the previous ensemble.

Calculations with $\nu_{OH} = 3$ were excluded due to the small number of reactions found for the original set of initial conditions (see Figure 4). Qualitatively, the reaction rates are comparable to those from simulations in which excitation of the equilibrium ensemble were used, see Figure 4. Also, the relative importance of direct HCl elimination and elimination preceded by H-transfer to neighboring oxygen atoms is comparable. Quantitatively, the decomposition probability for all excitation is reduced by 25% to 30% compared to simulations with initial conditions taken from *NVE* simulations. Furthermore, the reaction slows down, as can be seen by comparing, e.g., the point at which excitation with $\nu_{OH} = 6$ reaches 50% reactivity. For the results shown in Figure 6 with the alternative set of initial conditions, this occurs at around 1 ns compared to ≈ 500 ps for the original choice of initial conditions, see Figure 4. The same is found for the crossing point between direct and indirect elimination with $\nu_{OH} = 5$ and 6 which is shifted towards a longer times.

The trajectories run with the Monte Carlo initial conditions were analyzed in the same fashion as the original 5000 trajectories, see Figure S-IV (Supplementary Information). The energy distributions after HCl elimination are slightly shifted towards higher energies when compared to Figure 5. However, the distributions remain qualitatively similar. As for the vibrationally induced decomposition reaction, conclusions drawn from the final state analysis are robust with respect to the two very different procedures to generate initial conditions for the non-equilibrium simulations. For excitation with $\nu_{OH} = 4$ beating patterns are observed for both types of initial conditions (but particularly pronounced with those from Monte Carlo sampling). However, interpretation of those would be premature, also because the number of reactive trajectories for this level of excitation is only around 15 %.

The decomposition reactions preceded by intramolecular H-transfer differ from direct HCl elimination primarily by the time scale on which dissociation occurs, see Figures 4 and 6. In order to characterize the differences between these two reaction pathways, geometrical coordinates were sought which can can be used to further analyze indirect elimination. Visual inspection of the dynamics suggested that the H-Cl-S-O_A dihedral angle ϕ could be a meaningful choice. The dihedral angle ϕ can distinguish between the three oxygen atoms in a symmetric way (with O_A on the mirror axis). The distance O_A helps to further distinguish the reactive trajectories, especially with respect to the position of the hydrogen to its acceptor. The trajectories can be grouped into those in which during the dynamics the hydrogen atom binds to oxygen atoms O_A and O_B, O_A
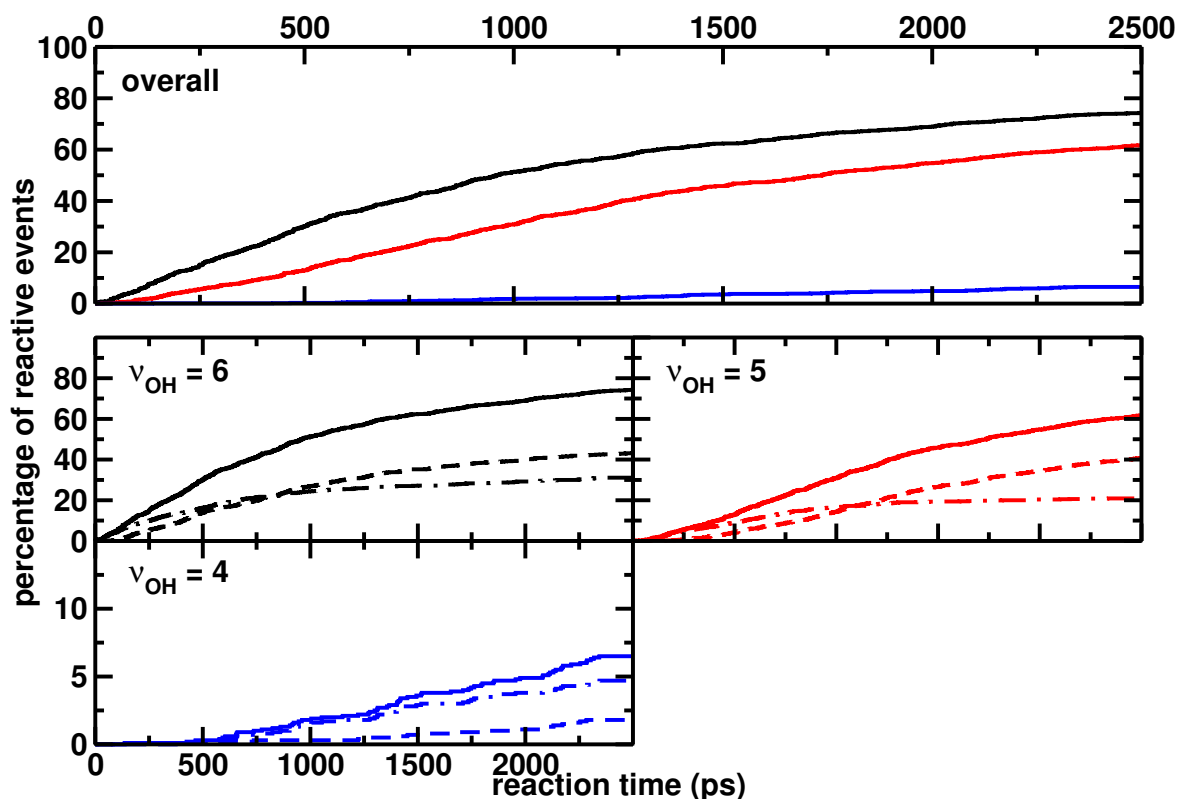
14

FIG. 6: Reaction kinetics from 1000 trajectories with initial conditions from the Monte Carlo sampling. Top panel) Total number of reactive events (direct HCl elimination + HCl elimination preceded by intramolecular H-transfer). Blue, red and black curves correspond to excitation of $\nu_{OH} = 4$, 5 and 6, respectively. Bottom panels) Total number of reactive events (solid), direct HCl elimination (dashed), and HCl elimination preceded by intramolecular H-transfer (dotted dashed) for $\nu_{OH} = 4$, 5 and 6 in the same color code as in the top panel.

and O_C, or to all three oxygen atoms.

Probability distributions $p(r_{HO_A}, \phi)$ from analyzing 1000 trajectories, taken from the ensemble in which excitation of the equilibrium was used, for each of the excitation levels are reported in Figure 7. Each column displays, from top to bottom, H-transfer to (I) both oxygen atoms, (II) O_B only, (III) O_C only before HCl elimination occurs. The columns report results for increasing number of OH-quanta from left to right. Each panel was individually normalized. For excitation with $\nu_{OH} = 4$ (left column) only a small number of trajectories show indirect HCl elimination:
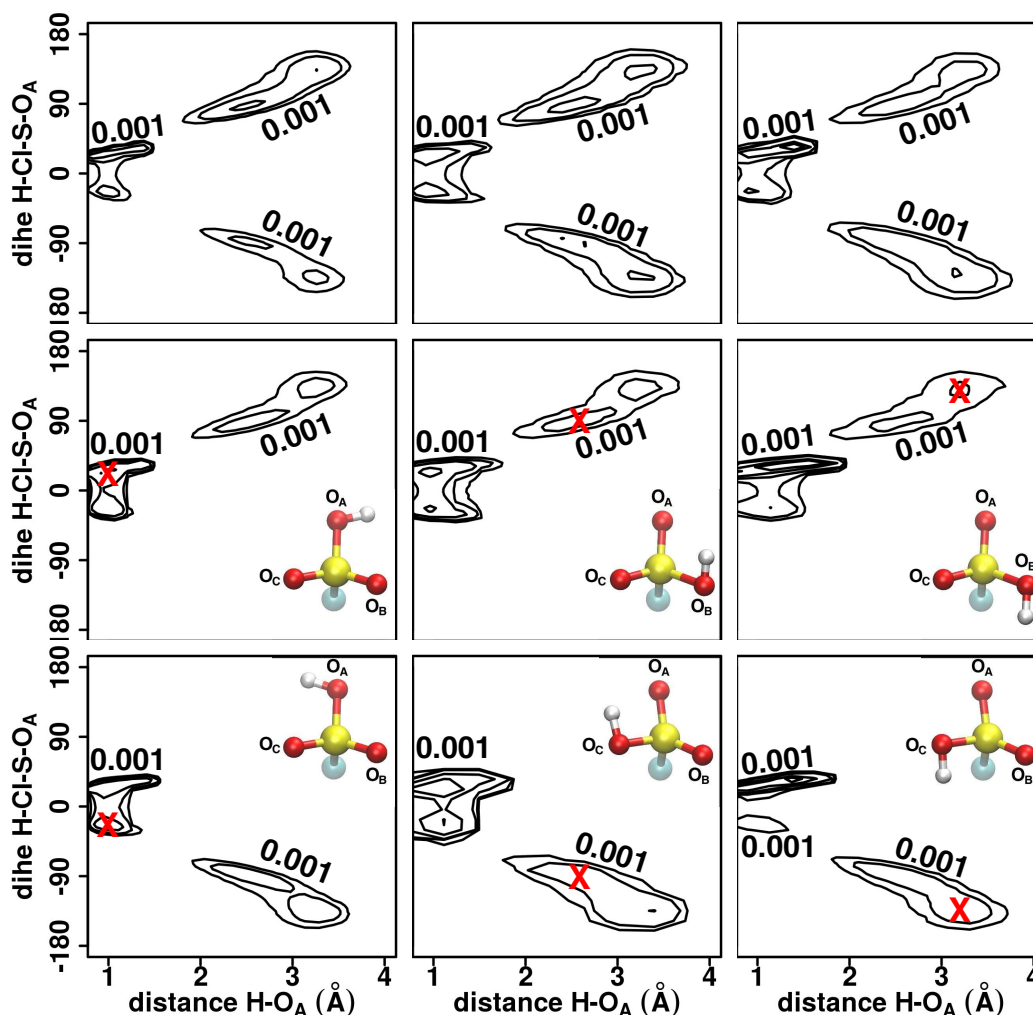
FIG. 7: Probability distribution $p(r_{\mathrm{HO_A}}, \phi)$, with ϕ as the dihedral angle between H-Cl-S-O_A, shown as contour lines. From left to right excitation with $\nu_{\mathrm{OH}} = 4$, 5, and 6. From top to bottom indirect trajectories showing H-transfer to both oxygen atoms, to O_B only, and to O_C only. The molecular structures represent the geometry of the region marked with a red cross (for each panel individually). $p(r_{\mathrm{HO_A}}, \phi)$ was normalized to unity for each panel and the lowest isocontour is labelled in each case.

for cases (I) to (III) there are 2, 39 and 10 events, respectively. For excitation with 5 quanta these numbers increase to 295, 525, and 104 trajectories whereas for excitation with $\nu_{\mathrm{OH}} = 6$ cases (I) to (III) occur for 356, 358, and 86 runs. Hence, for excitations with 4 to 6 quanta 90%, 10% and 20% of the trajectories, respectively, lead to HCl elimination without transfer between neighboring oxygen atoms.

16

The distribution of the angle ϕ reveals two states for each possible H-O$_X$ (X = A, B, C) bond, see red crosses with corresponding molecular models in Figure 7. These states correspond to two synperiplanar positions of the hydrogen with respect to O$_X$. The probability distributions for the two states at $\phi = \pm 25°$ and short HO$_A$ bond length consist of the positions of the hydrogen atom sampled a) in the equilibrium trajectories of HO$_A$SO$_2$Cl before excitation and b) during the migratory dynamics after vibrational excitation. This explains the high probabilities in these two positions. The distribution of the H-O$_A$ bond length broadens for higher vibrational excitations as the vibrational energy along the OH-bond increases (see left sides in the panels in Figure 7). With $\nu_{OH} = 4$ the hydrogen remains longer in a specific orientation since the HO$_A$S rotation barrier is rarely overcome. This – and the small number of trajectories in this class – leads to the asymmetric distribution along ϕ in the top left corner. For excitation with $\nu_{OH} = 5$ the distribution $p(r_{HO_A}, \phi)$ for trajectories sampling all oxygen atoms is most symmetrical. This indicates that the dihedral barrier can be overcome and that extensive sampling of all oxygen positions by the hydrogen atom is possible before elimination. Finally, with $\nu_{OH} = 6$ the distribution in the top right corner is again less symmetric as the residence time of the hydrogen on each oxygen before elimination is shortened due to the high excitation energy. The middle column of Figure 7 illustrates the increasing H-O$_A$ amplitude as the number of quanta is increased from left to right. From these probability distributions it is evident that coupling between the OH-stretching vibration and the torsional degrees of freedom is an essential pathway for energy exchange which influences the rates and yields of HCl elimination on the picosecond time scale.

IV. CONCLUSION

In summary, the present work establishes that vibrational excitation of OH-overtones with 3 to 6 quanta leads to HCl elimination on the sub-nanosecond to ns time scale for HSO$_3$Cl. For short times (a few hundred ps) after vibrational excitation this process is usually direct, i.e. without previous intramolecular H-transfer and leads to characteristic energy distributions in the diatomic fragment which should be experimentally detectable. Direct and indirect HCl elimination occur whereby the latter is driven by appreciable excitation of torsional degrees of freedom and dominates at longer times. It is shown that the conclusions from the simulations are

robust towards the particular choice of initial conditions. Experimentally corroborating such a reaction mechanism will be relevant for atmospheric chemistry at large, since under the conditions in the stratopause around the poles vibrationally excited states can survive sufficiently long for decomposition to occur. The reaction is fast (sub-ns to ns time scale) compared to collisionally induced quenching, which occurs on the hundred ns time scale.[18,33] Hence, there is only little competition for the dissociative channel. The present work provides testable hypotheses for experiments and establishes a vibrationally driven photodissociation mechanism for HSO_3Cl which is a meaningful proxy for H_2SO_4 relevant in atmospheric chemistry.

---

1 B. J. Finlayson-Pitts, Anal. Chem., 2010, **82**, 770–776.

2 D. J. Hofmann and J. M. Rosen, Nature, 1982, **297**, 120–124.

3 F. Raes, R. V. Dingenen, E. Vignati, J. Wilson, J.-P. Pataud, J. H. Seinfeld and P. Adams, Atmos. Environ., 2000, **34**, 4215 – 4240.

4 U. Pöschl, Angew. Chem. Int. Ed. Engl., 2005, **44**, 7520–7540.

5 R. Charlson, J. Lovelock, M. Andreae and S. Warren, Nature, 1987, **326**, 655 – 661.

6 R. Kiene, Nature, 1999, **402**, 363 – 368.

7 R. Simó and C. Pedrós-Alió, Nature, 1999, **402**, 396 – 399.

8 B. Huebert, Nature, 1999, **400**, 713 – 714.

9 K. Capaldo, J. Corbett, P. Kasibhatla, P. Fischbeck and S. Pandis, Nature, 1999, **400**, 743 – 746.

10 L. J. Larson, M. Kuno and F. M. Tao, J. Chem. Phys., 2000, **112**, 8830 – 8838.

11 F. C. Charles and J. F. Ian, Atmos. Environ., 1999, **33**, 1352 – 2310.

12 P. Rasch, S. Tilmes, R. Turco, A. Robock, L. Oman, C.-C. Chen, G. Stenchikov and R. Garcia, Philos.

Trans. R. Soc. Lond., A, 2008, **306**, 4007 – 4037.

13 K. Caldeira and L. Wood, Philos. Trans. R. Soc. Lond., A, 2008, **366**, 4039 – 4056.

14 D. J. Hofmann and J. M. Rosen, Geophys. Res. Lett., 1985, **12**, 13–16.

15 J. Zhao, O. B. Toon and R. P. Turco, J. Geophys. Res., D, 1995, **100**, 5215–5227.

16 C. P. Rinsland, M. R. Gunson, M. K. W. Ko, D. W. Weisenstein, R. Zander, M. C. Abrams, A. Goldman, N. D. Sze and G. K. Yue, Geophys. Res. Lett., 1995, **22**, 1109–1112.

17 M. J. Mills, O. B. Toon and S. Solomon, Geophys. Res. Lett., 1999, **26**, 1133–1136.

18 V. Vaida, H. G. Kjaergaard, P. E. Hintze and D. J. Donaldson, Science, 2003, **299**, 1566 – 1568.

19 J. B. Burkholder, M. Mills and S. McKeen, Geophys. Res. Lett., 2000, **27**, 2493–2496.

20 P. E. Hintze, H. G. Kjaergaard, V. Vaida and J. B. Burkholder, J. Chem. Phys., 2003, **107**, 1112 – 1118.

21 S. J. Wrenn, L. J. Butler, G. A. Rowland, C. J. Knox and L. F. Phillips, J. Chem. Phys., 1999, **129**, 1112 – 1118.

22 H. G. Kjaergaard, J. R. Lane, A. L. Garden, D. P. Schofield, T. W. Robinson and M. Mills, Adv. Quantum Chem., 2008, **55**, 1112 – 1118.

23 T. W. Robinson, D. P. Schofield and H. G. Kjaergaard, J. Chem. Phys., 2003, **118**, 7226 – 7232.

24 J. R. Lane and H. G. Kjaergaard, J. Phys. Chem. A, 2008, **112**, 4958 – 4964.

25 F. F. Crim, Annu. Rev. Phys. Chem., 1984, **35**, 657 – 691.

26 T. Uzer, J. Hynes and W. Reinhardt, J. Chem. Phys., 1986, **85**, 5791–5804.

27 F. F. Crim, J. Phys. Chem., 1996, **100**, 12725–12734.

28 D. K. Havey, K. J. Feierabend and V. Vaida, J. Mol. Struct-Theochem, 2004, **680**, 243 – 247.

29 J. R. Lane, H. G. Kjaergaard, K. L. Plath and V. Vaida, J. Phys. Chem. A, 2007, **111**, 5434 – 5440.

30 P. E. Hintze, K. J. Feierabend, D. K. Havey and V. Vaida, Spec. Acta A-Mol. Biomol. Spec., 2005, **61**, 559 – 566.

31 K. J. Feierabend, D. K. Havey, S. S. Brown and V. Vaida, Chem. Phys. Lett., 2006, **420**, 438 – 442.

32 J. Yosa and M. Meuwly, J. Phys. Chem. A, 2011, **115**, 14350 – 14360.

33 J. Yosa, T. Nagy and M. Meuwly, Phys. Chem. Chem. Phys., 2014, **16**, 18533 – 18544.

34 P. Gupta, J. R. Lane and H. G. Kjaergaard, Phys. Chem. Chem. Phys., 2010, **12**, 8277–8284.

35 J. R. Lane and H. G. Kjaergaard, J. Phys. Chem. A, 2007, **111**, 9707–9713.

36 T. Nagy, J. Yosa and M. Meuwly, J. Chem. Theory. Comput., 2014, **10**, 1366 – 1375.

37 M. J. Frisch, G. W. Trucks, H. B. Schlegel, G. E. Scuseria, M. A. Robb, J. R. Cheeseman, G. Scalmani, V. Barone, B. Mennucci, G. A. Petersson, H. Nakatsuji, M. Caricato, X. Li, H. P. Hratchian, A. F. Iz-

maylov, J. Bloino, G. Zheng, J. L. Sonnenberg, M. Hada, M. Ehara, K. Toyota, R. Fukuda, J. Hasegawa, M. Ishida, T. Nakajima, Y. Honda, O. Kitao, H. Nakai, T. Vreven, J. A. Montgomery, Jr., J. E. Peralta, F. Ogliaro, M. Bearpark, J. J. Heyd, E. Brothers, K. N. Kudin, V. N. Staroverov, R. Kobayashi, J. Normand, K. Raghavachari, A. Rendell, J. C. Burant, S. S. Iyengar, J. Tomasi, M. Cossi, N. Rega, J. M. Millam, M. Klene, J. E. Knox, J. B. Cross, V. Bakken, C. Adamo, J. Jaramillo, R. Gomperts, R. E. Stratmann, O. Yazyev, A. J. Austin, R. Cammi, C. Pomelli, J. W. Ochterski, R. L. Martin, K. Morokuma, V. G. Zakrzewski, G. A. Voth, P. Salvador, J. J. Dannenberg, S. Dapprich, A. D. Daniels, Ö. Farkas, J. B. Foresman, J. V. Ortiz, J. Cioslowski and D. J. Fox, Gaussian 09 Revision D.01, Gaussian Inc. Wallingford CT 2009.

38 S. M. Chackalackal and F. E. Stafford, J. Am. Chem. Soc., 1966, **88**, 4815–4819.

39 T. Shimanouchi, Tables of molecular vibrational frequencies. Consolidated volume II, 1977, `http://link.aip.org/link/JPCRBU/v6/i3/p993/s1{\&}Agg=doi`.

40 B. R. Brooks, C. L. Brooks, III, A. D. Mackerell, Jr., L. Nilsson, R. J. Petrella, B. Roux, Y. Won, G. Archontis, C. Bartels, S. Boresch, A. Caflisch, L. Caves, Q. Cui, A. R. Dinner, M. Feig, S. Fischer, J. Gao, M. Hodoscek, W. Im, K. Kuczera, T. Lazaridis, J. Ma, V. Ovchinnikov, E. Paci, R. W. Pastor, C. B. Post, J. Z. Pu, M. Schaefer, B. Tidor, R. M. Venable, H. L. Woodcock, X. Wu, W. Yang, D. M. York and M. Karplus, J. Chem. Comp., 2009, **30**, 1545–1614.

41 M. Meuwly, A. Müller and S. Leutwyler, Phys. Chem. Chem. Phys., 2003, **5**, 2663–2672.

42 P. N. Nguyen and G. Stock, J. Chem. Phys., 2003, **119**, 11350–11358.

43 M. P. Grubb, M. L. Warter, H. Xiao, S. Maeda, K. Morokuma and S. W. North, Science, 2012, **335**, 1075–1079.

44 L. Bonnet and J. Rayez, Chem. Phys. Lett., 1997, **277**, 183–190.

45 H. Schranz, S. Nordholm and G. Nyman, J. Chem. Phys., 1991, **94**, 1487–1498.

46 N. Metropolis, A. W. Rosenbluth, M. N. Rosenbluth, A. H. Teller and E. Teller, J. Chem. Phys., 1953, **21**, 1087–1092.